www.springer.com/41230
https://doi.org/10.1007/s41230-026-5091-8
Research & Development
Vol. 23 No. 4 July 2026
CHINA FOUNDRY

Effect of heat treatment on microstructure, mechanical, antibacterial and corrosion properties of cast TC4-4.34Cu titanium alloy

***Wei-long Wang[1, 2], Yan-chun Lou[1], Hong-yu Liu[1, 2], Shi-bing Liu[1, 2], Kun Shi[1, 2], Hong-ju Li[1, 2], Xian-yu Bao[2], and Jia-shuo Zhang[1, 2]**

1. State Key Laboratory of Advanced Casting Technologies, Shenyang 110022, China

2. Shenyang Research Institute of Foundry Co., Ltd. CAM, Shenyang 110022, China

Abstract: The TC4-4.34Cu titanium alloy was prepared by water-cooled copper crucible vacuum suspension melting technology, followed by hot isostatic pressing at 920 °C under 130 MPa. Subsequently, heat treatments were conducted at 720 °C and 800 °C, respectively. The microstructures of the alloy were analyzed using X-ray diffraction, scanning electron microscopy, and transmission electron microscopy equipped with an energy dispersive spectrometer, and its mechanical properties, antibacterial performance, and corrosion resistance were evaluated. Results show that cast TC4-4.34Cu alloy matrix consists of α-phase, β-phase, and Ti_2Cu phase. However, numerous porosity defects lead to a low plasticity of the alloy. Hot isostatic pressing effectively eliminates porosities and improves the densification of the alloy. Heat treatment at 720 °C promotes a more uniform and denser alloy matrix microstructure, yielding optimal mechanical properties, specifically, a tensile strength of 944 MPa and an elongation of 7%. In contrast, heat treatment at 800 °C causes the Ti_2Cu phase to coarsen and increases the volume fraction and size of the β phase, resulting in a sharp decline in plasticity and brittle fracture. Antibacterial and corrosion resistance tests reveal that compared to TC4 alloy, the TC4-4.34Cu alloy exhibits excellent antibacterial properties due to the sustained release of Cu^{2+} ions, which effectively inhibits bacterial membrane growth in *P.aeruginosa* solution. The antibacterial rate of the TC4-4.34Cu alloy after heat treatment at 720 °C reaches 83%. Additionally, the improved impedance value of the TC4-4.34Cu alloy enhances its corrosion resistance.

Keywords: cast TC4-Cu alloy; mechanical properties; antimicrobial properties; corrosion resistance

CLC numbers: TG146.23 **Document code:** A **Article ID:** 1672-6421(2026)04-535-09

1 Introduction

Titanium alloys, known as "marine metals", are widely recognized as one of the most promising materials for marine engineering applications. Their excellent specific strength and corrosion resistance significantly enhance the performance and durability of structural components[1-5]. However, their excellent biocompatibility makes titanium alloys susceptible to microbiologically influenced corrosion during service in marine environments, thereby reducing the service life of titanium alloy components[6-8]. It has been reported that adding elements with antimicrobial properties, such as Cu or Ag, to titanium alloys can effectively improve their antibacterial capabilities[9-16]. However, the high cost of Ag makes it impractical for extensive use in engineering structural applications. Therefore, the low-cost and high antimicrobial capacity of Cu element can be well applied on marine engineering titanium alloys.

Ti-Cu and TC4-Cu alloys prepared by forging[17-20], laser additive manufacturing[21, 22] and sintering[23, 24], have good mechanical properties and excellent antibacterial performance, showing great application potential in the medical field. However, for large, heavy, and complex titanium alloy structural components used in marine engineering, conventional methods such as forging, laser additive manufacturing, or sintering are unsuitable for overall production. In comparison, casting has significant advantages in overall forming. It can ensure the uniformity of the internal structure

***Wei-long Wang**

Male, doctoral candidate. His research primarily focuses on corrosion and wear resistant materials, and composition design of titanium alloys.

E-mail: 15140179842@163.com

Received: 2025-04-16; Revised: 2025-08-01; Accepted: 2025-11-04

of the component while reducing the adverse effects caused by splicing and welding. However, the mechanical properties of cast Ti-Cu and TC4-Cu alloys are not satisfactory[25-29]. Kikuchi et al.[25] studied the mechanical properties of cast Ti-Cu alloys with Cu content ranging from 1% to 10%, observing that the elongation decreased from 7% to 1% as the Cu content increased. Aoki et al.[26] studied the mechanical properties of cast TC4-*x*Cu (*x*=1%, 4%, and 10%) alloys and found that the elongation was only 0.2% to 2.8%, and the fracture mode was brittle fracture. For titanium alloy castings with complex geometries, heat treatment serves as an effective means of property optimization. Ma et al.[19] demonstrated that heat treatment at 930 °C optimizes the mechanical performance of Ti6Al4V-5Cu alloy. Peng et al.[20] showed that annealing can modulate the volume fraction of the Ti_2Cu phase in Ti6Al4V-*x*Cu alloys, thereby improving their mechanical properties. For cast TC4-Cu components intended for marine service, excellent mechanical properties are a prerequisite for safe operation. Therefore, enhancing the mechanical properties of TC4-Cu alloy castings through heat treatment is critical to ensuring their safe service in marine environments.

In this work, a vacuum induction suspension melting furnace was used to prepare a TC4-4.34Cu alloy. By applying different heat treatment processes, the effects of heat treatment on the mechanical properties, antibacterial performance, and corrosion resistance of the TC4-4.34Cu alloy were investigated. This work aims to provide a basis optimizing for the comprehensive properties of Cu-containing cast titanium alloys.

2 Experimental materials and methods

The TC4-4.34Cu alloy was prepared using sponge Ti, Al45V55, pure Al, and pure Cu as raw materials, and melted in a 10 kg vacuum induction suspension melting furnace. To ensure uniform composition, each alloy ingot was melted three times, with each melting lasting 10 min. After melting, the alloy was poured into a metal mold. Specimens were taken from the finished ingot for composition analysis, and the results (mass fraction, wt.%) are: Al 5.43, V 3.91, Cu 4.34, N 0.01, O 0.02, H 0.01, with Ti is the balance. The specimens in the cast state were referred to as Cast. The phase transformation points of the TC4-4.34Cu alloy were determined to be 765 °C and 865 °C using a simultaneous thermal analyzer (STA 449F3, GER). According to the Ti-Cu phase diagram in Fig. 1, they are the phase transformation points of α+Ti_2Cu to β and α to β, respectively. The ingot was then subjected to hot isostatic pressing at 920 °C (β phase region) and 130 MPa for 2 h using a hot isostatic pressing device (QIH1200, China), and the corresponding specimens were referred to HIP. The ingots after hot isostatic pressing were subjected to vacuum heat treatment at 720 °C (α+Ti_2Cu phase region) and 800 °C (α+β phase region) for 1 h using a vacuum heat treatment furnace (ZCL1250, China), and cooled with argon gas, the corresponding specimens were referred to as HIP-720 and HIP-800, respectively. In addition, the cast TC4 alloy subjected to hot isostatic pressing was used as a reference specimen, referred to as TC4. Microbiological corrosion experiments were conducted together with HIP and HIP-720 specimens.

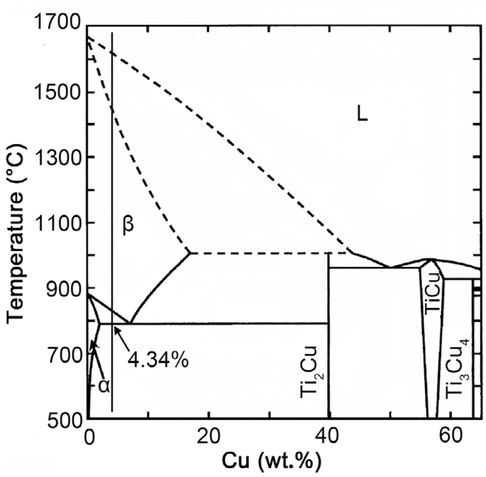

Fig. 1: Ti-Cu binary phase diagram[30]

The phase constitution of the alloys was identified by X-ray diffraction (Smart Lab, Japan) using Cu Kα radiation with a scan rate of 5°·min^{-1}. The microstructures were observed by a scanning electron microscope (JSM-7001F, Japan). Microstructure morphology observation and compositional analysis were carried out using a transmission electron microscope (JEM-F200, Japan) equipped with an energy dispersive spectrometer (EDS). The phase volume fraction and size in the alloy were detected using Image-Pro Plus software. Mechanical properties were tested using a universal electronic testing machine (DDL300, China) with a tensile rate of 0.9 mm·min^{-1}. The specimens were round bar tensile specimens with a parallel section diameter of 5 mm and M10 threads at both ends.

The antibacterial experiments were conducted in accordance with the GB/T2591 standard, using *P.aeruginosa*, a common marine bacterium. A bacterial suspension of 50 μL with a concentration of 1.0×10^5 cfu·mL^{-1} was added to the specimen surface and incubated at 30 °C for 24 h.

After incubation, the specimens were immersed in 2 mL of 3.5% NaCl solution to dilute the bacterial suspension. Then, 100 μL of the diluted suspension was spread onto nutrient 2216E agar plates and incubated for an additional 24 h before counting the bacterial colonies. The antibacterial rate (R) was calculated using Eq. (1) to evaluate the antibacterial performance of the material:

$$R(\%) = \frac{N_{control} - N_{experiment}}{N_{control}} \times 100\% \quad (1)$$

where $N_{control}$ is the average number of bacteria on the control specimen, and $N_{experiment}$ is the average number of bacteria on the experimental specimen. Live/dead bacterial staining assays were used to observe bacterial biofilms. A bacterial suspension of 50 μL with a concentration of 1.0×10^6 cfu·mL^{-1} was added to the specimen surface and incubated at 30 °C for 24 h. After incubation, the bacterial suspension was gently aspirated, and the adherent bacteria on the specimen surface were stained with SYTO®9 (5 mmol·L^{-1}, green fluorescence) and PI (30 mmol·L^{-1}, red fluorescence) for 30 min, followed by observation under a fluorescence microscope (OLYMPUS/DP80, Japan). The experimental data were represented as mean values with standard deviations, and the results of the live/dead bacterial staining assays were analyzed using SPSS 13.0 software, with significant differences expressed as p<0.05.

Specimens were immersed in a solution containing *P.aeruginosa* at a concentration of 1.0×10^5 cfu·mL^{-1} and maintained at 30 °C for 10 days. Subsequently, electrochemical experiments were conducted using an electrochemical workstation (VersaSTAT 3F, USA). The electrochemical cell employed a standard three-electrode system, with a Pt sheet as the counter electrode, a saturated calomel electrode as the reference electrode, and the immersed specimen (solution contact area=1 cm^2) as the working electrode. The solution used was a 1% *P.aeruginosa* suspension, and the solution temperature was maintained at 30 °C during the experiment. Before the experiment, the specimens were soaked in the solution for 30 min to achieve a stable open-circuit potential. The electrochemical impedance spectra (EIS) were measured by applying a sinusoidal potential perturbation of 5 mV with frequency from 10^{-2} Hz to 10^5 Hz in logarithmic increment at open circuit potential. Potentiodynamic polarization curves were recorded within a potential range of −1.0 V to +1.0 V at a scan rate of 5 mV·s^{-1}. An X-ray photoelectron spectrometer (Model Axis Supra+, Japan) was used to analyze the composition and valence of the corrosion products on the alloy specimens. To guarantee the accuracy of the test data, in this work, the specimens used in the tensile, antibacterial, and corrosion experiments were each subjected to three repeated tests.

3 Results

Figure 2 shows the XRD patterns of TC4-4.34Cu alloy in different states. The cast specimen consists of α-phase, β-phase, and Ti_2Cu phase, with no detection of Cu or Ti_3Cu peaks, indicating Cu fully dissolves into the alloy to form Ti_2Cu phases. The weakened intensity of the Ti_2Cu phase peaks of the HIP specimens proves that the content of Ti_2Cu phase is reduced by the hot isostatic pressing at 920 °C. The Ti_2Cu phase peak intensity of HIP-720 specimen is enhanced, indicating that the heat treatment in the α+Ti_2Cu phase region promotes the precipitation of Ti_2Cu phase. During heat treatment in the α+β phase region, the HIP-800 specimen undergoes a transformation from α+Ti_2Cu to β, resulting in a significantly increased intensity of the β-Ti peak. However, due to the short holding time in the α+β phase region, the Ti_2Cu phase does not fully dissolve into the alloy, and Ti_2Cu peaks are still present in the XRD patterns.

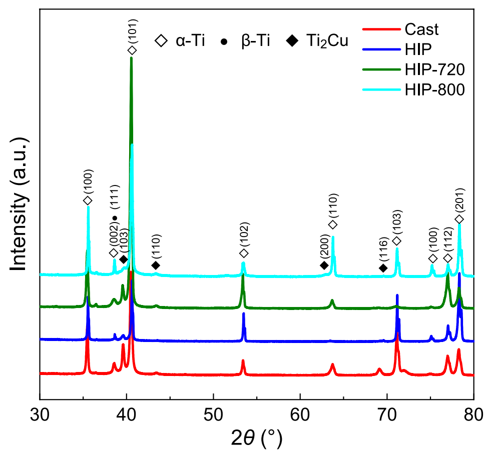

Fig. 2: XRD patterns of TC4-4.34Cu alloy in different states (Cast, HIP, HIP-720, and HIP-800)

Figure 3 shows microstructures of TC4-4.34Cu alloy in different states. In the cast state [Fig. 3(a)], gas holes are distributed in the matrix, and discontinuous α-phase is present within the β-phase. As shown in Fig. 3(b), after hot isostatic pressing, the internal gas hole of the alloy is eliminated, resulting in a uniform and dense structure. A portion of the β-phase decomposes into acicular α-phase. Bright white particles are scattered on the alloy matrix, which are assumed to be Ti_2Cu phase based on the XRD results. Figure 3(c) shows the microstructure of the HIP-720 specimen. The acicular α-phase transforms into lamellar α-phase, which is uniformly distributed in the β-Ti matrix. The Ti_2Cu phase precipitates and grows, distributing at the α/β interfaces and within the β-phase, leading to a more uniform microstructure. Figure 3(d) shows the microstructure of the HIP-800 specimen. The lamellar α-phase is isolated and dispersed, while the β-phase becomes larger and forms a continuous distribution. The volume fraction increases significantly to 32.40%. A small amount of large-sized Ti_2Cu phase is observed at the α/β interface.

Figure 4(a) shows the microstructure of the HIP specimen, with the granular phases enriched at the α/β interfaces and within the β-phase. Figure 4(b) shows the selected area electron diffraction (SAED) pattern of the granular phase in Fig. 4(a), and the corresponding EDS quantitative analysis results (Region A) are shown in Table 1. The analysis results indicate that the granular precipitates are Ti_2Cu phase, which has a tetragonal crystal structure (a=0.29438 nm, c=1.0786 nm)[31]. Figures 4(c) and (f) show the surface scan results for Regions D and F, respectively, and these are combined with the elemental content of each area in Table 1. It can be concluded that the bright white and dark black granular phases observed in the HIP [Fig. 4(a)], HIP-720 [Fig. 4(d)], and HIP-800 [Fig. 4(e)] specimens are all Ti_2Cu phases. Furthermore, the results indicate that the Ti_2Cu phase contains 39.21wt.% Cu, 0.61wt.% Al, and 0.91wt.% V. In contrast, the α-phase contains 8.62wt.% Al with very low levels of V and Cu. Compared to the α-phase, the β-phase has higher Cu and V contents but lower Al content; and the content of Cu in the β-phase increases with the increase of heat treatment temperature. This further confirms that Cu and V are β-stabilizing elements, while Al is an α-stabilizing element. At the same time, increasing the heat treatment temperature also led to changes in the size of the Ti_2Cu phase. The sizes of the Ti_2Cu phase in the three heat-treated specimens are approximately 400, 650, and 950 nm, respectively. This is because the heat treatment of the α+Ti_2Cu

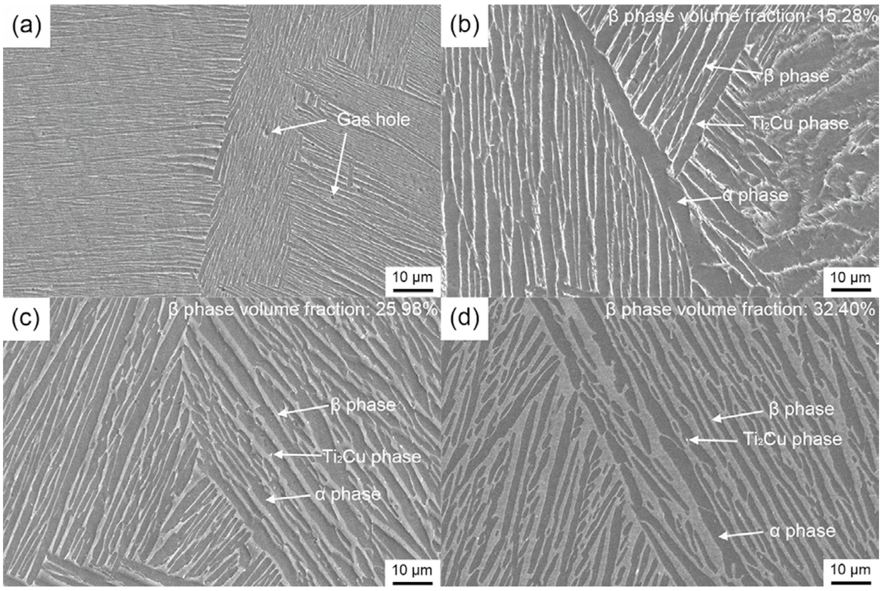

Fig. 3: Microstructures of TC4-4.34Cu alloy in different states: (a) Cast; (b) HIP; (c) HIP-720; (d) HIP-800

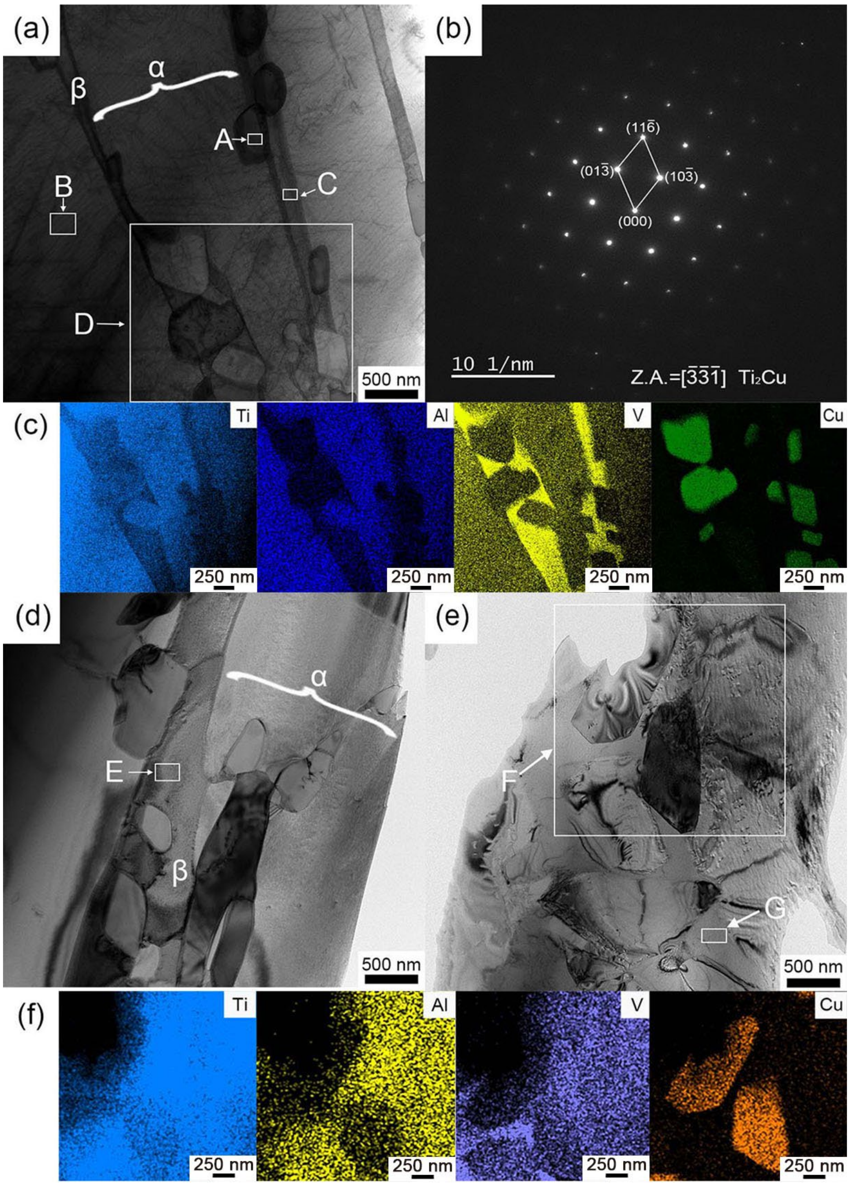

Fig. 4: TEM images and EDS analysis of TC4-4.34Cu alloy in different states: (a) HIP; (b) SAED pattern taken from Area A in (a); (c) EDS pattern taken from Area D in (a); (d) HIP-720; (e) HIP-800; (f) EDS pattern taken from Area F in (e)

Table 1: Element content at different regions in Fig. 4 (wt.%)

Regions	Cu	Al	V	Ti
A	39.21	0.61	0.91	59.27
B	1.79	8.62	0.95	88.64
C	3.95	1.72	12.76	81.57
D	10.15	3.88	6.39	79.58
E	4.23	1.60	19.95	74.22
F	20.23	4.32	6.43	69.02
G	6.23	1.56	12.39	79.82

phase region causes coarsening of Ti_2Cu phases. Subsequently, during heat treatment in the α+β phase region, Ostwald ripening causes these Ti_2Cu phases to coarsen further, resulting in a continuous increase in size[32, 33].

Figure 5 shows the mechanical behavior of TC4-4.34Cu alloy in different states. The Cast specimen has the highest tensile strength of 1,060 MPa, while the tensile strength of HIP-720 specimen is the lowest, but it still reaches 944 MPa. The tensile strengths of the specimens, in ascending order, are HIP-720<HIP<HIP-800<Cast. The elongation results indicate that the Cast and HIP-800 specimens have low elongation of about 2%, showing brittle fracture. The HIP-720 specimen has the highest elongation of 7%, indicating a transition from brittle to ductile fracture. The elongations of the specimens, in ascending order, are Cast<HIP-800<HIP<HIP-720.

Figure 6 shows the antibacterial results of TC4 and different TC4-4.34Cu alloys cultured in *P.aeruginosa* for 24 h. As shown in Fig. 6(a), the TC4 alloy surface exhibits abundant bacterial growth. Figures 6(b) and (c) indicate that the bacterial colonies on the TC4-4.34Cu alloy are significantly reduced after copper addition. Compared to the control alloy TC4, the HIP specimen has a 70% antibacterial rate, while the HIP-720 specimen achieves the highest rate of 83%.

Figure 7 shows the results of live/dead bacterial staining and biofilm thickness on the surfaces of TC4 and TC4-4.34Cu alloys after 24 h of bacterial culture. The green areas indicate live bacteria, while the red areas indicate dead bacteria. Figure 7(a) shows that the biofilm on the TC4 alloy surface is densely populated with live bacteria, with almost no dead cells observed. Figures 7(b) and (c) show that the TC4-4.34Cu alloy surfaces exhibit a sparse distribution of live bacteria, accompanied by a large number of red-stained dead bacteria. Figures 7(d), (e), and (f) represent the biofilm thickness of the three specimens. The biofilm on the TC4 alloy is the thickest at 18.23 μm, while the HIP and HIP-720 specimens exhibit biofilm thicknesses of 11.70 and 9.16 μm, respectively. This indicates that adding Cu to the TC4 alloy significantly reduces biofilm thickness, further confirming that the TC4-4.34Cu alloy effectively inhibits bacterial biofilm formation and growth.

Figure 8 shows the electrochemical curves of TC4 and TC4-4.34Cu alloys after immersion in bacterial solution for 10 days. Figure 8(a) shows the Nyquist plots of the three specimens. The arc in the Nyquist plot reflects the charge transfer process at the electrode surface, with the arc radius indicating the electron transfer resistance. The larger the radius, the greater the transfer resistance on the electrode surface, the

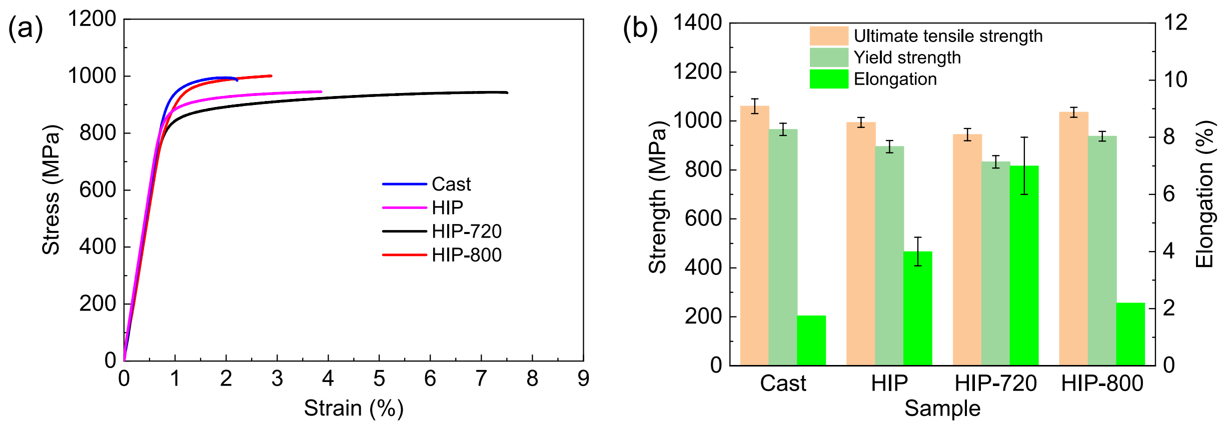

Fig. 5: Mechanical behavior of TC4-4.34Cu alloy in different states: (a) stress-strain curves; (b) performance data

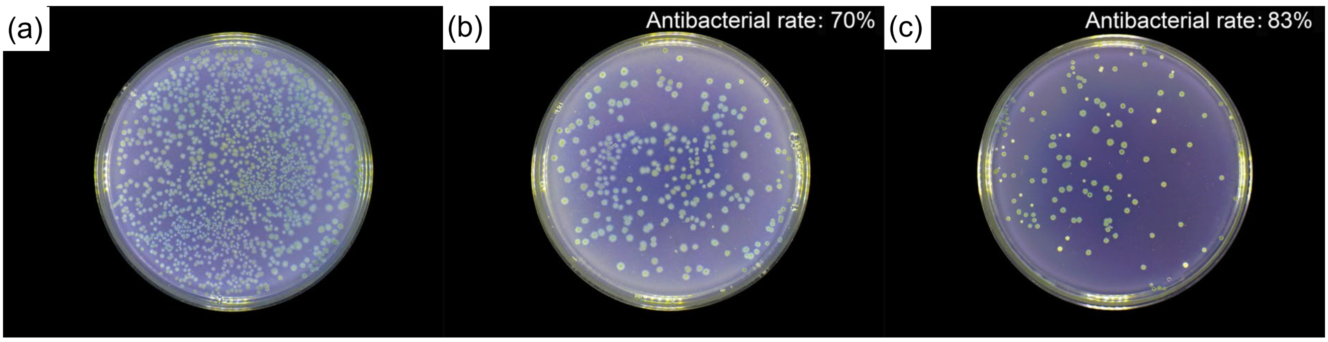

Fig. 6: Results of antimicrobial tests on TC4 (a) and TC4-4.34Cu (b and c) alloys: (a) TC4; (b) HIP; (c) HIP-720

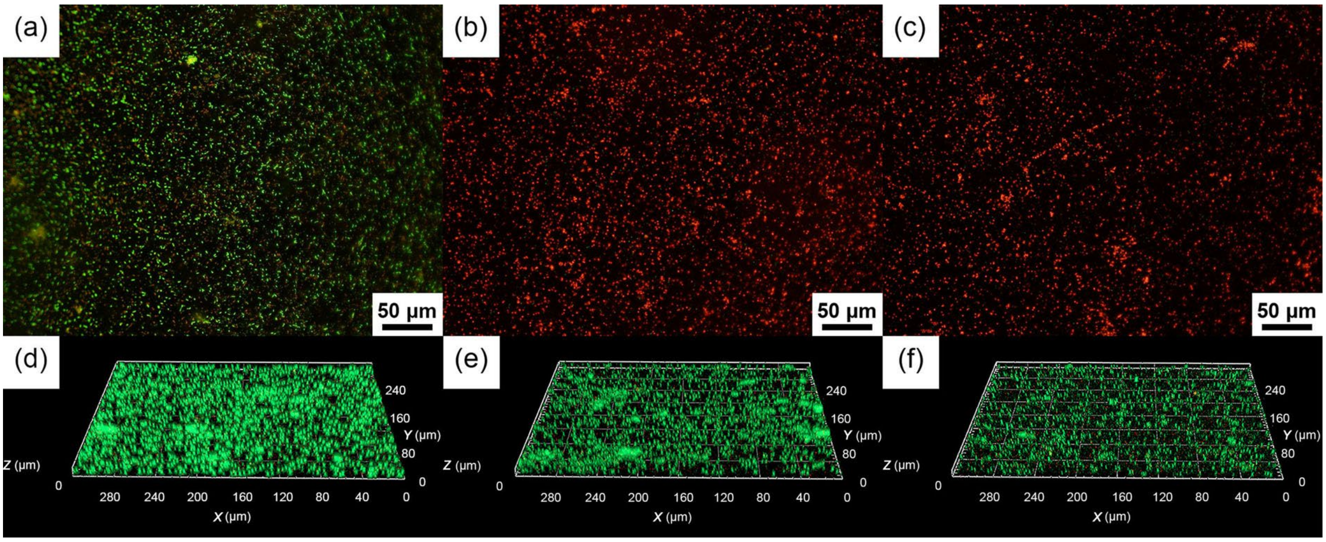

Fig. 7: Results of live/dead bacterial staining (a–c) and biofilm thickness (d–f) experiments on TC4 and TC4-4.34Cu alloys: (a, d) TC4; (b, e) HIP; (c, f) HIP-720

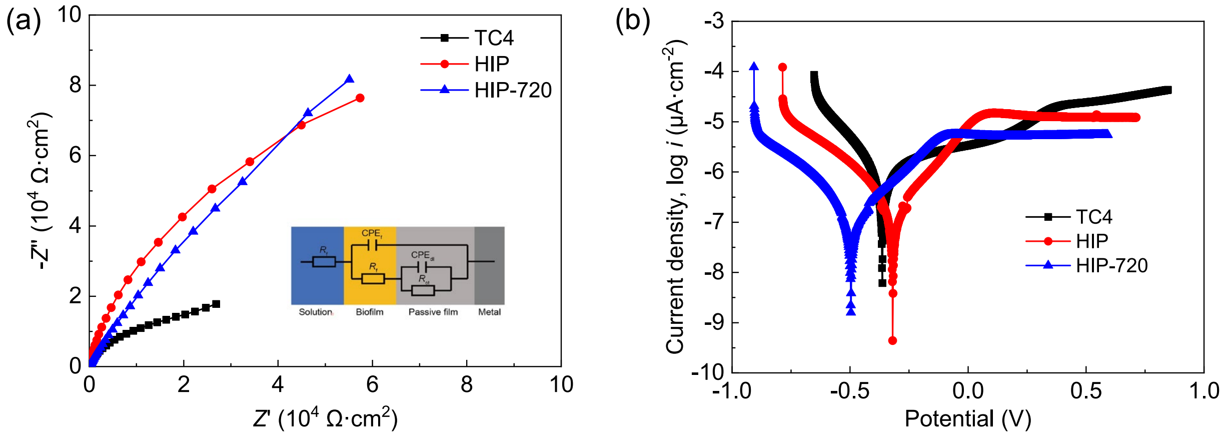

Fig. 8: Electrochemical profiles of TC4 alloy and TC4-4.34Cu alloy specimens after immersion incubation: (a) Nyquist plots; (b) potentiodynamic polarization curves

larger the impedance of the electrode surface, and the better the corrosion resistance. The TC4-4.34Cu alloy has a much larger arc radius than the TC4 alloy. The equivalent circuit $R(Q(R(QR)))$ was used for fitting, and the fitted parameters are shown in Table 2. R_s, R_f, and R_{ct} represent the resistances of the bacterial solution, the biofilm, and the passive film on the alloy surface, respectively. CPE_f and CPE_{dl} represent the constant phase elements of the biofilm and the passive film, respectively. Their n values both fall within the range of 0.8–1, indicating near-ideal capacitive behavior.The impedance of the passive film of the TC4-4.34Cu alloy is one order of magnitude higher than that of the TC4 alloy. Figure 8(b) shows the potentiodynamic polarization curves, from which the corrosion potential (E_{corr}) and corrosion current density (i_{corr}) are obtained. E_{corr} reflects the corrosion tendency of the alloy but not the corrosion rate. Thus, i_{corr} was used to characterize the corrosion resistance. The i_{corr} value of the TC4-4.34Cu alloy specimens is lower than that of the TC4 alloy, indicating that Cu addition enhances corrosion resistance. Among the specimens with different heat treatments, the HIP-720 specimen exhibits the lowest i_{corr}, showing the best corrosion resistance.

Table 2: Electrochemical parameters of TC4 alloy and TC4-4.34Cu alloy specimens after immersion incubation

Specimens	R_s (Ω·cm^2)	CPE_f (10^{-8} S·s^n)	R_f (10^3 Ω·cm^2)	n	CPE_{dl} (10^{-5} S·s^n)	R_{ct} (10^4 Ω·cm^2)	n	i_{corr} (μA·cm^{-2})	E_{corr} (V)
TC4	2.89	36.72	37.26	0.98	8.27	3.30	0.86	95.41	−0.36
HIP (TC4-4.34Cu)	2.69	0.03	35.47	0.87	10.21	17.42	0.90	15.12	−0.32
HIP-720 (TC4-4.34Cu)	3.54	0.23	22.45	0.96	6.07	23.82	0.93	10.75	−0.50

4 Analysis and discussion

Figure 9 shows the fracture morphology of the TC4-4.34Cu alloy in different states at room temperature. Figure 9(a) shows that the fracture morphology of the Cast specimen consists of large cleavage planes, indicating a brittle fracture mechanism. In contrast, the fracture morphology of the HIP specimen [Fig. 9(b)] consists of a mixed morphology formed by numerous small ductile dimples and tear edges, indicating a ductile fracture mechanism. As shown in Fig. 9(c), the fracture characteristics of the HIP-720 specimen are similar to those of the HIP specimen. However, there are more ductile dimples and fewer cleavage planes, giving the HIP-720 specimen excellent plasticity. The fracture surface morphology of the HIP-800 specimen consists of cleavage planes accompanied by a small number of tear edges. As illustrated in Fig. 9(d), the fracture mechanism is a mixed ductile-brittle type, and the alloy exhibits low plasticity.

The course as-cast microstructures and large porosity defects present in the Cast specimens are the main causes of brittle fracture. Following hot isostatic pressing, the porosity defects within the alloy are effectively eliminated. This is accompanied by a phase transformation from the β-phase to the α-phase, as well as the precipitation of the Ti_2Cu phase. These fine Ti_2Cu particles hinder the subsequent deformation of the alloy by impeding the slip and climb motion of dislocations. Following the α+Ti_2Cu phase region heat treatment of the HIP specimen, the size of the Ti_2Cu phase increases. But the alloy's overall microstructural uniformity and density are improved. The optimal balance of strength and ductility is achieved through the combined effects of a uniform microstructure and relatively fine Ti_2Cu particles. However, after α+β phase region heat treatment of the HIP specimen, the Ti_2Cu phase undergoes significant coarsening (~950 nm). At the same time, some of the Ti_2Cu phases dissolve, releasing Cu elements which stabilize the β phase. This promotes an increase in the volume fraction of the β phase and an expansion of its layer width. Ultimately, the coarse Ti_2Cu phase and the high-volume fraction of the β phase cause brittle fracture in the HIP-800 specimen.

Figure 10 shows the XPS spectra of TC4 and HIP-720 specimens after 10 days of culture in bacterial solution. Both TC4 and HIP-720 specimens show Ti^{4+} and O^{2-} ion precipitation on their surfaces, indicating the formation of a TiO_2 passive film that hinders further erosion of the alloy substrate by the bacterial solution. However, Cu^{2+} ions are detected on the surface of the HIP-720 specimen, and their formation mechanism is as follows[34]:

$$O_2+H_2O+4e^-\rightarrow 4OH^- \quad (2)$$

$$Ti_2Cu+8OH^-\rightarrow 2TiO_2+Cu^{2+}+4H_2O+10e^- \quad (3)$$

The O_2 in the reaction originates from the bacterial solution, while the e^- are produced during the extracellular electron transfer of *P. aeruginosa* as it survives and metabolizes. Through the reactions described in Eqs. (2) and (3), the Ti_2Cu phase in the TC4-4.34Cu alloy undergoes hydrolysis to generate Cu^{2+} ions, which possess antibacterial properties. The precipitation of Cu^{2+} ions is crucial for the excellent antibacterial performance and inhibition of bacterial biofilm growth in the TC4-4.34Cu alloy. Additionally, the HIP-720 specimen exhibits better antibacterial effects than the HIP specimen. This is attributed to the promotion of Ti_2Cu phase precipitation during the α+Ti_2Cu phase region heat treatment. The HIP-720 specimen has a larger size and higher content of the Ti_2Cu phase compared to other specimens, resulting in the optimal antibacterial performance.

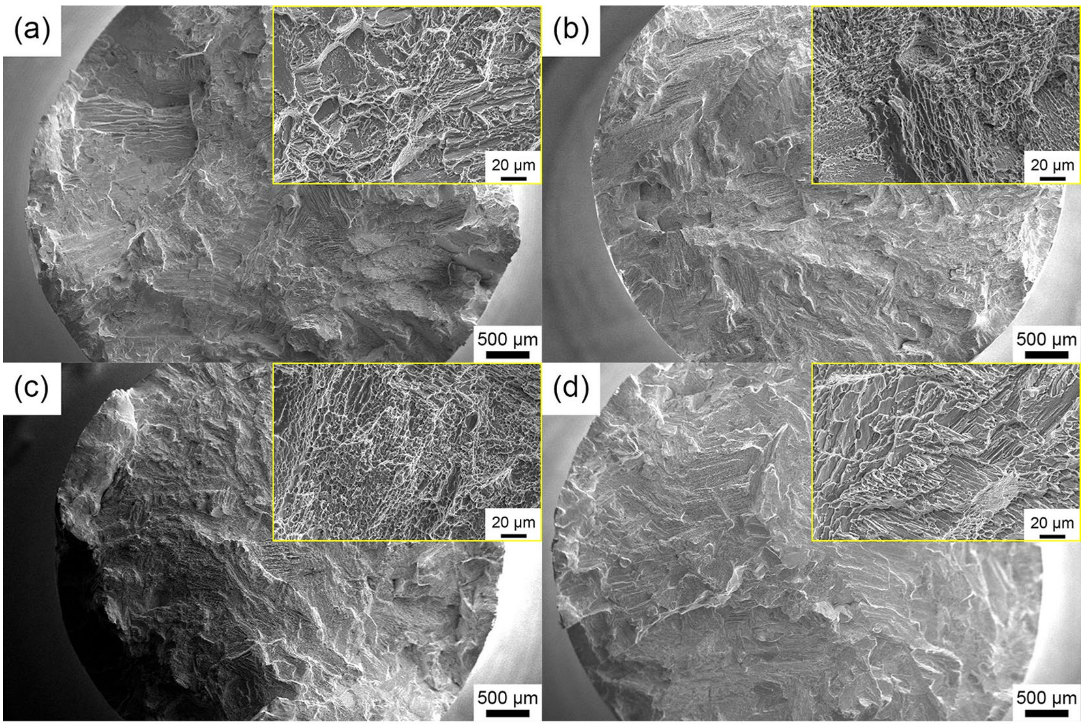

Fig. 9: Fracture morphology of TC4-4.34Cu alloy in different states: (a) Cast; (b) HIP; (c) HIP-720; (d) HIP-800

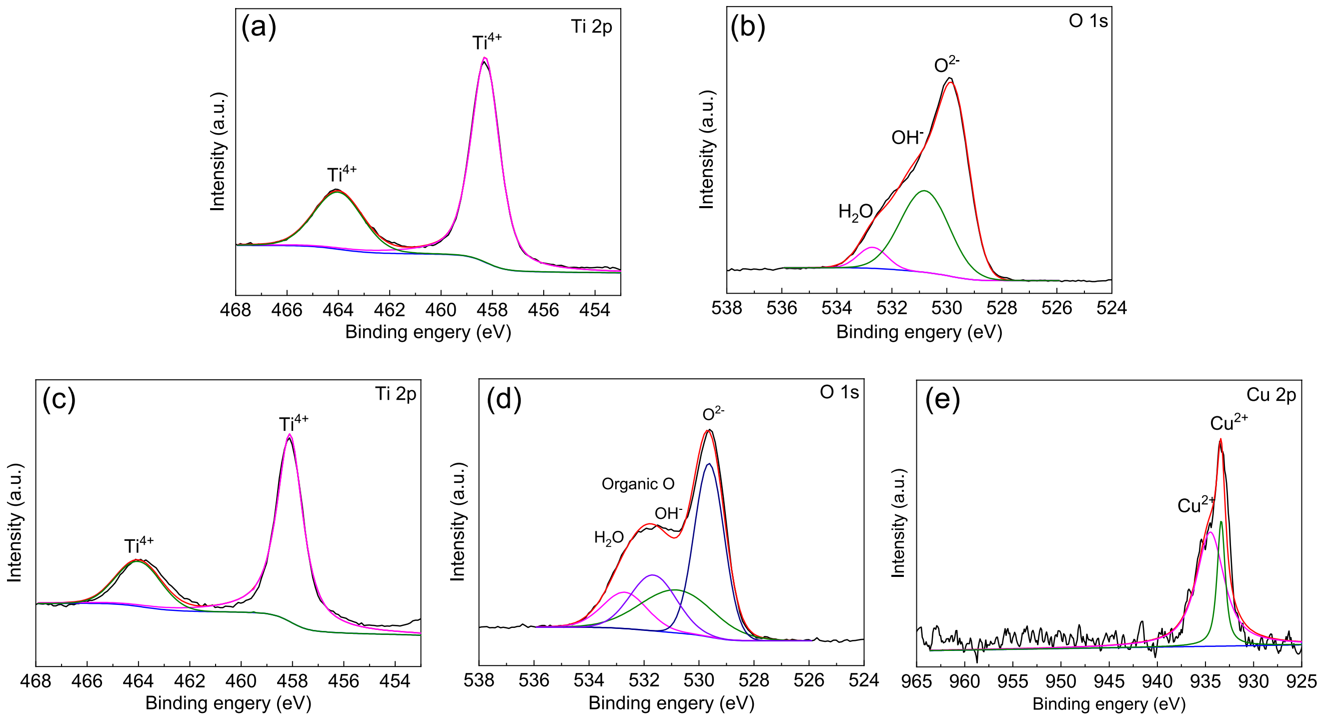

Fig. 10: PS profiles of the specimen surfaces of TC4 and HIP-720 specimens after 10 days of incubation in bacterial-containing solution: (a) Ti 2p mapping of TC4 specimen; (b) O 1s mapping of TC4 specimen; (c) Ti 2p mapping of HIP-720; (d) O 1s mapping of HIP-720; (e) Cu 2p mapping of HIP-720

The polarisation curve test results of TC4-4.34Cu alloy show that the addition of Cu improves the corrosion resistance of the alloy. As a β-stabilizing element, Cu promotes β-phase formation in the alloy. The increase in β-phase raises the electron transfer resistance and reduces the dissolution rate of alloy elements.

The HIP-720 specimen exhibits better corrosion resistance than the TC4 specimen. This is attributed to the addition of Cu, which decreases the volume fraction of the α-phase and increases the β-phase in the TC4-4.34Cu alloy.

5 Conclusions

Different heat treatment temperatures lead to varied microstructures in the TC4-4.34Cu alloy, thereby affecting its mechanical properties, antimicrobial properties, and corrosion resistance.

(1) The microstructure of TC4-4.34Cu alloy consists of α-phase, β-phase, and Ti_2Cu phase. After heat treatment at 720 °C, lamellar α-phase and large Ti_2Cu particles form in the alloy, which give it optimal comprehensive mechanical properties. However, heat treatment at 800 °C induces coarsening of the β-phase and remelting of the Ti_2Cu phase, which increases strength but severely reduces plasticity, ultimately resulting in brittle fracture.

(2) Compared to the TC4 alloy, the TC4-4.34Cu alloy releases Cu^{2+} ions in *P.aeruginosa* solution, effectively suppressing bacterial biofilm growth and enhancing antibacterial performance. The TC4-4.34Cu alloy subjected to heat treatment at 720 °C achieves an 83% antibacterial rate, with its impedance is one order of magnitude higher than that of the TC4 alloy, indicating superior corrosion resistance.

Acknowledgments

This work was financially supported by the Joint Fund Project General support program of Liaoning Province (Grant No. 2023-MSLH-339) and the Liaoning Province “unveiled the leader” project (Grant No. 22016225ZK01).

Conflict of interest

The authors declare that they have no conflict of interest.

References

[1] Cui C X, Hu B M, Zhao L C, et al. Titanium alloy production technology, market prospects and industry development. Materials & Design, 2011, 32(3): 1684–1691.

[2] Yan S K, Song G L, Li Z X, et al. A state-of-the-art review on passivation and biofouling of Ti and its alloys in marine environments. Journal of Materials Science & Technology, 2018, 34(3): 421–435.

[3] Nady H, El-Rabiei M M, Samy M. Corrosion behavior and electrochemical properties of carbon steel, commercial pure titanium, copper and copper-aluminum-nickel alloy in 3.5% sodium chloride containing sulfide ions. Egyptian Journal of Petroleum, 2017, 26(1): 79–94.

[4] Kappenthuler S, Seeger S. Holistic evaluation of the suitability of metal alloys for sustainable marine construction from a technical, economic and availability perspective. Ocean Engineering, 2021, 219: 108378.

[5] Wang W L, Cui W F, Xiao Z T, et al. The improved corrosion and wear properties of Ti-Zr based alloys with oxide coating in simulated seawater environment. Surface and Coatings Technology, 2022, 439: 128415.

[6] Li Y F, Ning C Y. Latest research progress of marine microbiological corrosion and bio-fouling, and new approaches of marine anti-corrosion and anti-fouling. Bioactive Materials, 2019, 4: 189–195.

[7] Lou Y T, Chang W W, Cui T Y, et al. Microbiologically influenced corrosion inhibition mechanisms in corrosion protection: A review. Bioelectrochemistry, 2021, 141: 107883.

[8] Xiao Z T, Wang W L, Cui W F, et al. Marine microbial corrosion inhibitation of an in situ formed oxide coating on Ti56Zr44 alloy. Materials Chemistry and Physics, 2023, 304: 127924.

[9] Song C H, Chen Y Q, Liu L, et al. In situ alloying Ti-Ag antibacterial biomaterials via laser powder bed fusion: Microstructure, mechanical properties and bioperformance. Materials Today Advances, 2023, 20: 100445.

[10] Cai D G, Yu Z M, Yang L, et al. Effect of Ag content on the microstructure and antibacterial activity of biomedical titanium alloy Ti-13Nb-13Zr-*x*Ag (*x*=7, 10 wt.%). Materials Letters, 2024, 354: 135389.

[11] Arroussi M, Jia Q, Bai C G, et al. Inhibition effect on microbiologically influenced corrosion of Ti-6Al-4V-5Cu alloy against marine bacterium Pseudomonas aeruginosa. Journal of Materials Science & Technology, 2022, 109: 282–296.

[12] Zhang Y, Wang X Y, Ma Z L, et al. A potential strategy for in-stent restenosis: Inhibition of migration and proliferation of vascular smooth muscle cells by Cu ion. Materials Science and Engineering: C, 2020, 115: 111090.

[13] Zhang E L, Wang X Y, Chen M, et al. Effect of the existing form of Cu element on the mechanical properties, bio-corrosion and antibacterial properties of Ti-Cu alloys for biomedical application. Materials Science and Engineering: C, 2016, 69: 1210–1221.

[14] Hu J L, Li H X, Wang X Y, et al. Effect of ultrasonic micro-arc oxidation on the antibacterial properties and cell biocompatibility of Ti-Cu alloy for biomedical application. Materials Science and Engineering: C, 2020, 115: 110921.

[15] Lu M, Zhang Z M, Zhang J Q, et al. Enhanced antibacterial activity of Ti-Cu alloy by selective acid etching. Surface and Coatings Technology, 2021, 421: 127478.

[16] Takahashi M, Kikuchi M, Takada Y, et al. Mechanical properties and microstructures of dental cast Ti-Ag and Ti-Cu alloys. Dental Materials Journal, 2002, 21(3): 270–280.

[17] Arroussi M, Bai C G, Zhao J L, et al. Preliminary study on biocorrosion inhibition effect of Ti-5Cu alloy against marine bacterium Pseudomonas aeruginosa. Applied Surface Science, 2022, 578: 151981.

[18] Liu R, Memarzadeh K, Chang B, et al. Antibacterial effect of copper-bearing titanium alloy (Ti-Cu) against streptococcus mutans and porphyromonas gingivalis. Scientific Reports, 2016, 6(1): 29985.

[19] Ma Z, Ren L, Liu R, et al. Effect of heat treatment on Cu distribution, antibacterial performance and cytotoxicity of Ti-6Al-4V-5Cu alloy. Journal of Materials Science & Technology, 2015, 31(7): 723–732.

[20] Peng C, Liu Y, Liu H, et al. Optimization of annealing treatment and comprehensive properties of Cu-containing Ti6Al4V-*x*Cu alloys. Journal of Materials Science & Technology, 2019, 35(10): 2121–2131.

[21] Ju J, Zan R, Shen Z, et al. Remarkable bioactivity, bio-tribological, antibacterial, and anti-corrosion properties in a Ti-6Al-4V-*x*Cu alloy by laser powder bed fusion for superior biomedical implant applications. Chemical Engineering Journal, 2023, 471: 144656.

[22] Zhu M Z, Miao J L, Zhou X W, et al. Corrosion resistance and antibacterial properties of Ti-3Cu alloy prepared by selective laser melting. Transactions of Nonferrous Metals Society of China, 2025, 35(1): 143–156.

[23] Liu J, Li F B, Liu C, et al. Effect of Cu content on the antibacterial activity of titanium-copper sintered alloys. Materials Science and Engineering: C, 2014, 35: 392–400.

[24] Tao X W, Xia J Q, Xu Y T, et al. Role of Cu content in microstructure, mechanical, corrosion, tribological and antibacterial behavior of spark plasma sintered Ti-B-*x*Cu alloys for dental application. Vacuum, 2024, 222: 113085.

[25] Kikuchi M, Takada Y, Kiyosue S, et al. Mechanical properties and microstructures of cast Ti-Cu alloys. Dental Materials, 2003, 19(3): 174–181.

[26] Aoki T, Okafor I C I, Watanabe I, et al. Mechanical properties of cast Ti-6Al-4V-*x*Cu alloys. Journal of Oral Rehabilitation, 2004, 31(11): 1109–1114.

[27] Xu Q, Li W, Yin Y J, et al. Finite element simulation of real cavity closure in cast Ti6Al4V alloy during hot isostatic pressing. China Foundry, 2022, 19(1): 55–62.

[28] Wang Z, Fu B G, Wang Y F, et al. Effect of Cu content on the precipitation behaviors, mechanical and corrosion properties of as-cast Ti-Cu alloys. Materials, 2022, 15(5): 1696.

[29] Kerealme S, Bai C G, Jia Q, et al. Effect of annealing temperature on as-cast Ti6Al4V-5Cu alloy microstructure, tensile properties, and fracture toughness. Materials Today Communications, 2022, 33: 104508.

[30] Dyal Ukabhai K, Curle U A, Masia N D E, et al. Formation of Ti_2Cu in Ti-Cu alloys. Journal of Phase Equilibria and Diffusion, 2022, 43(3): 332–344.

[31] Donthula H, Vishwanadh B, Alam T, et al. Morphological evolution of transformation products and eutectoid transformation(s) in a hyper-eutectoid Ti-12at.% Cu alloy. Acta Materialia, 2019, 168: 63–75.

[32] Jiang C P, Zhang L X, Chen Y N, et al. Coarsening behavior of the Ti_2Cu phase of a Ti-14Cu alloy during isothermal thermal exposure. Journal of Alloys and Compounds, 2021, 882: 160685.

[33] Akbarpour M R, Mirabad H M, Hemmati A, et al. Processing and microstructure of Ti-Cu binary alloys: A comprehensive review. Progress in Materials Science, 2022, 127: 100933.

[34] Xin C, Wang N, Chen Y, et al. Biological corrosion behaviour and antibacterial properties of Ti-Cu alloy with different Ti_2Cu morphologies for dental applications. Materials & Design, 2022, 215: 110540.